THE ASTROPHYSICAL JOURNAL, 381:200–209, 1991 November 1

PRELIMINARY SPECTRAL OBSERVATIONS OF THE GALAXY WITH A 7° BEAM BY THE *COSMIC BACKGROUND EXPLORER (COBE)*[1]

E. L. WRIGHT,[2] J. C. MATHER,[3] C. L. BENNETT,[3] E. S. CHENG,[3] R. A. SHAFER,[3] D. J. FIXSEN,[4] R. E. EPLEE, JR.,[5] R. B. ISAACMAN,[5] S. M. READ,[6] N. W. BOGGESS,[3] S. GULKIS,[7] M. G. HAUSER,[3] M. JANSSEN,[7] T. KELSALL,[3] P. M. LUBIN,[8] S. S. MEYER,[9] S. H. MOSELEY, JR.,[3] T. L. MURDOCK,[10] R. F. SILVERBERG,[3] G. F. SMOOT,[11] R. WEISS,[9] AND D. T. WILKINSON[12]

Received 1991 February 21; accepted 1991 May 6

ABSTRACT

The far-infrared absolute spectrophotometer (FIRAS) on the *Cosmic Background Explorer* (*COBE*) has carried out the first all-sky spectral line survey in the far-infrared region, as well as mapping spectra of the Galactic dust distribution at $\lambda > 100$ μm. Lines of [C I], [C II], [N II], and CO are all clearly detected, [C II] (158 μm) and [N II] (205.3 μm) with sufficient strength to be mapped, and the wavelength of the [N II] line at 205.3 μm is determined by observation for the first time. The mean line intensities are interpreted in terms of the heating and cooling of the multiple phases of the interstellar gas. In addition, an average spectrum of the galaxy is constructed and searched for weak lines. The spectrum of the galaxy observed by FIRAS has two major components: a continuous spectrum due to interstellar dust heated by starlight with a total luminosity of $(1.8 \pm 0.6)(R_0/8.5\ \mathrm{kpc})^2 \times 10^{10}\ L_\odot$ within the solar circle; and a line spectrum dominated by the strong 158 μm line from singly ionized carbon, with a spatial distribution similar to the dust distribution, and a luminosity of 0.3% of the dust luminosity. There are in addition moderately strong 122 and 205.3 μm lines, identified as coming from singly ionized nitrogen, which contribute 0.04% and 0.03% of the total dust luminosity. The much weaker lines of neutral carbon at 370 and 609 μm are seen, as are the 2–1 through 5–4 CO lines. These low-J CO lines contribute 0.003% of the total dust luminosity. Maps of the emission by dust, [C II], and [N II] are presented.

Subject headings: infrared: spectra — interstellar: grains — interstellar: matter — interstellar: molecules

1. INTRODUCTION

The far-infrared absolute spectrophotometer (FIRAS) on the *Cosmic Background Explorer* (*COBE*) offers a unique capability to measure the absolute flux from our galaxy in the millimeter and submillimeter bands unencumbered by atmospheric and instrument emission. Although the instrument has an angular resolution of only 7° and is therefore not suited to the traditional mode of detailed mapping, it is an effective instrument to measure the absolute diffuse emission from the galaxy. Also, because of its almost two decades of spectral coverage with moderate spectral resolution, it serves to take an unbiased inventory of the stronger spectral lines and dust emission emanating from the Galaxy.

Field, Goldsmith, & Habing (1969) proposed that the interstellar medium (ISM) would have multiple stable equilibrium phases. McKee & Ostriker (1977) expanded on this model, introducing four phases of the ISM. McKee & Ostriker maintain that most space is filled by a hot ionized medium (HIM), while most of the mass is in a cold neutral medium (CNM). Surrounding clouds of the CNM are coronae of warm neutral medium (WNM) and warm ionized medium (WIM). The importance of the WIM is emphasized in the review by Kulkarni & Heiles (1986), but to date the WIM has been seen only in diffuse Hα emission (Reynolds 1984), several optical metastable lines such as diffuse [N II] ($\lambda\lambda$6583.4, 6548,1) and [S II] (λ6716) emission (Reynolds, Roesler, & Scherb 1977), high-n radio recombination lines (Lockman 1976), and pulsar dispersion measures. Tielens & Hollenbach (1985) realized that many lines were radiated primarily from the interface region between the CNM and the WNM, and made detailed models of what they called a photodissociation region (PDR), which includes all of the WNM and most of the CNM.

While the bulk of the far-infrared emission from the Galaxy is a continuous spectrum from interstellar dust heated by starlight, the gaseous phase of the interstellar medium produces sharp spectral lines. The cooling model for the interstellar medium has long predicted that the dominant heat loss mechanism for the gas is the 158 μm line of [C II] (Dalgarno & McCray 1972). Since carbon is the most abundant atom with an ionization potential (11.26 eV) less than that of hydrogen, and since [C II] has an easily excited fine structure state only 91 K above the ground state, most of the heat added to the cool neutral phase of the interstellar gas will ultimately be radiated at 158 μm. One expects that far-IR continuum produced by grains will follow the [C II] emission because the

[1] The National Aeronautics and Space Administration/Goddard Space Flight Center (NASA/GSFC) is responsible for the design, development, and operation of the *Cosmic Background Explorer* (*COBE*). Scientific guidance is provided by the *COBE* Science Working Group. GSFC is also responsible for the development of the analysis software and for the production of the mission data sets.

[2] UCLA Astronomy Department, Los Angeles, CA 90024-1562.
[3] NASA Goddard Space Flight Center, Code 685, Greenbelt, MD 20771.
[4] University Space Research Assoc., Code 610.3, NASA/GSFC, Greenbelt, MD 20771.
[5] General Sciences Corporation, Code 685, NASA/GSFC, Greenbelt, MD 20771.
[6] ST Systems Corporation, 4400 Forbes Blvd., Lanham, MD 20706.
[7] Jet Propulsion Laboratory, Pasadena, CA 91109.
[8] UCSB Physics Department, Santa Barbara, CA 93106.
[9] MIT Department of Physics, Room 20F-001, Cambridge, MA 02139.
[10] General Research Corporation, 5 Cherry Hill Drive, Danvers, MA 01923.
[11] LBL & SSL, Bldg 50-351, University of California, Berkeley, CA 94720.
[12] Princeton University Department of Physics, Princeton, NJ 08540.

dominant source of heat for the interstellar gas is provided by photoelectrons ejected from grains by UV photons (Watson 1972). The ratio of [C II] to dust emission will be modulated by factors relating to the grain cross sections, the color of the interstellar radiation field, and the charge of the dust grain, which will be sufficiently positive in regions of high-UV flux and low gas density to suppress the emission of photoelectrons.

Russell et al. (1980) first observed the 158 μm line, and later this group mapped it in many sources. As expected, the line emission covered a large angular extent. This made the measurement of total line luminosities difficult with a warm, spatially chopped telescope. Stacey et al. (1983b) estimated the total flux of the 158 μm line by using the Moon as a reference with zero line flux during an occultation of the Galactic plane. Crawford et al. (1985) observed external galaxies and found the [C II] line emits about 0.5% of the bolometric far-infrared luminosity in M82, NGC 1068, and M83. Recently Stacey et al. (1991) have published [C II] line fluxes for a total of 20 galaxies, including normal spirals, infrared luminous peculiar galaxies such as NGC 6240 and M82, and active galaxies such as NGC 1068 and NGC 5128, and get a median ratio of L[C II]/L(FIR) of 0.29% with first and third quartiles at 0.15% and 0.4%.

Lines from neutral carbon are seen from the more opaque parts of the interstellar medium. Neutral carbon has two submillimeter fine structure transitions. The first astrophysical detections of the 609 μm $^3P_1$–$^3P_0$ transition of [C I] and the 370 μm $^3P_2$–$^3P_1$ transition of [C I] were made by Phillips et al. (1980) and Jaffe et al. (1985), respectively. Jaffe et al. concluded that the [C I] emission most likely arises from the edges of molecular clouds where UV heating is significant: the PDR modeled by Tielens & Hollenbach (1985). Recent reviews of PDR models and their confrontation with observations are in Genzel (1991) and Genzel, Harris, & Stutzki (1989).

Many other lines have been observed in the far-infrared and submillimeter spectrum using the Kuiper Airborne Observatory (KAO) and ground-based millimeter-wave telescopes. One line which has been sought using airborne telescopes is the "204" μm line of [N II]. The other transition in the triplet ground state of [N II] at 122 μm has recently been observed by Rubin et al. (1989). The optical lines of [N II] from the diffuse ISM have been observed by Reynolds et al. (1977), but interstellar extinction obscures our view of most of the Galaxy in these lines. The KAO is not able to study the strong submillimeter lines connected to the ground states of ortho and para water, or the submillimeter lines of molecular oxygen, because of the large column density of these molecules in the Earth's atmosphere.

The sharp lines arising from the gaseous phase of the ISM are only a small part of the radiation from dust. The far-infrared continuum emission from the Galaxy was first detected by Hoffman & Frederick (1969) using a 2.5 cm diameter balloon-borne telescope with a 2°.3 beam. They found a far-infrared luminosity greater than $7 \times 10^8\ L_\odot$. This pioneering work has been extended by Low et al. (1977), by Gispert, Puget, & Serra (1982) who gave a luminosity of $2 \times 10^{10}\ L_\odot$, and by Hauser et al (1984) who gave 1–2 $\times 10^{10}\ L_\odot$ for the luminosity within the solar circle. However, most of these maps have used spatial chopping to cancel the large thermal emission from warm telescopes. They thus may have underestimated the global emission from the Galaxy. Most of the subsequent effort has gone into increasing the spatial resolution of the Galactic maps. *IRAS* produced a map of the Galaxy without using a spatial chopper, but the zero level of the flux was uncertain. In addition, the DC-coupled detectors on *IRAS* exhibited an "AC-DC" nonlinearity (frequency dependent gain that depends on intensity and history) that makes the calibration for large-scale structure differ from the point source calibration. Hauser et al. (1989, 1991) found large scale-factor discrepancy at the largest angular scales in the *IRAS* 60 and 100 μm data, with preliminary data from the *COBE* DIRBE experiment requiring a significant bolometric correction. Furthermore, the longest wavelength *IRAS* band at 100 μm is shorter than the peak of Galactic dust emission as determined from the data reported in this paper. Hence, previous estimates of the total far-IR luminosity of the Galaxy have suffered from many uncertainties.

In this paper we present observations of nine far-infrared lines from four species: [C II] which comes from the CNM, WNM, and WIM in the McKee & Ostriker (1977) picture; [N II] which comes from the WIM; and [C I] and CO which come from the CNM and WNM (or PDR). We derive the flux averaged over the Galaxy for each of these components. Table 1 gives the fluxes for the lines we observed, as well as limits on lines from H_2O, O_2, [O I], and [S I].

We also present the weighted average spectrum of interstellar dust heated by starlight in our galaxy as measured by FIRAS, using the same weights that were used to determine the line fluxes in Table 1.

2. INSTRUMENT AND OBSERVATIONS

The FIRAS instrument on *COBE* has a 7° FWHM beam and gives fluxes that are referenced in flight to a movable precision external blackbody calibrator. The spectral range covered by FIRAS is nominally from 1 to 100 cm^{-1}, which just covers the spectral peak of the Galactic dust emission. The FIRAS instrument is a Michelson interferometer that uses bolometers for detectors and is thus ideally suited for a luminosity census of the interstellar medium, in addition to its primary goal of precise measurements of the spectrum of the cosmic background (Mather et al. 1990). The FIRAS beam shape has steep sides and is established by a compound parabolic concentrator, or Winston cone.

The FIRAS has four scan modes available: two scan lengths and two scan speeds. The data discussed here were taken in either the long-fast (LF) mode or the short-slow (SS) mode. The apodized spectral resolution in short-scan data is 0.7 cm^{-1} FWHM. In the LF mode, the low-frequency channel achieves higher spectral resolution (0.18 cm^{-1}). The high-frequency channel does not normally achieve higher resolution in the long scans due to telemetry limitations. However, some special observations were made where the short section of the long scan that could be recorded in the high-frequency channel was offset from the center of the interferogram. An inflight calibration of the frequency scale of the FIRAS has been derived from observations of the 2–1 through 5–4 CO lines, the [C I] line at 492.1612 GHz (Zmuidzinas et al 1988), and the [C II] line at 1900.5369 GHz (Boreiko, Betz, & Zmuidzinas 1988). The frequency calibration appears to be accurate to one part in 3000, based on the consistency of the fit to known lines.

The instrument data are processed in several steps. The raw interferograms are averaged while removing glitches caused by cosmic rays hitting the detectors. The interferograms are Fourier transformed into spectra and divided by the known electronic and digital filter transfer functions, and by the detector responsivitity calculated from its operating point. These

TABLE 1

LINE FLUXES IN THE AVERAGE SPECTRUM[a]

ν (cm^{-1})	λ (μm)	Species	Transition	Flux/10^{-8} (ergs s^{-1} cm^{-2} sr^{-1})	log L ($L_\odot$)
3.845[b]	2601.	CO	$J = 1$–0	0.6 ± 0.7	...
7.681	**1302.**	**CO**	**$J = 2$–1**	**2.8 ± 0.4**	**4.9**
11.531	**867.2**	**CO**	**$J = 3$–2**	**3.9 ± 0.9**	**5.1**
14.168[b]	705.8	O_2	$N_J = 3_2$–1_2	−0.7 ± 0.7	...
15.375	**650.4**	**CO**	**$J = 4$–3**	**4.2 ± 0.9**	**4.1**
16.419	**609.1**	**[C I]**	**$2p^2:{}^3P_1$–$^3P_0$**	**6.4 ± 1.3**	**5.3**
18.576[b]	538.3	H_2O	$J_{K_pK_0} = 1_{10}$–1_{01}	−0.3 ± 0.5	...
19.237	**519.8**	**CO**	**$J = 5$–4**	**3.1 ± 0.9**	**5.0**
23.06[b]	433.7	CO	$J = 6$–5	−5.7 ± 11.	...
27.00	**370.4**	**[C I]**	**$2p^2:{}^3P_2$–$^3P_1$**	**11.6 ± 1.6**	**5.5**
37.136[b]	269.3	H_2O	$J_{K_pK_0} = 1_{11}$–0_{00}	−2.3 ± 2.2	...
48.72	**205.3**	**[N II]**	**$2p^2:{}^3P_1$–$^3P_0$**	**166 ± 9**	**6.7**
63.395	**157.7**	**[C II]**	**$2p:{}^2P_{3/2}$–$^2P_{1/2}$**	**1726 ± 70**	**7.7**
68.716[b]	145.5	[O I]	$2p^4:{}^3P_0$–$^3P_1$	41 ± 23	...
77.11[b]	129.7	[Si I]	$3p^2:{}^3P_1$–$^3P_0$	38 ± 47	...
82.04	**121.9**	**[N II]**	**$2p^2:{}^3P_2$–$^3P_1$**	**261 ± 36**	**6.9**

[a] Detections are in bold face.
[b] Assumed frequency for nondetections.

spectra are transformed back into interferograms, apodized, extended with zeros, and retransformed into spectra. Then the spectra are divided by the optical responsivitity, determined from the response to the external calibrator at known temperatures, and adjustments are made for the emissions from the instrument. These emissions were determined from spectra taken with the external calibrator, the internal reference body, and the horn antennas at a variety of temperature combinations from 2 to 25 K. In order to obtain calibrations at high frequencies the external calibrator and the internal reference body must both be heated to close to their maximum temperatures. Unfortunately the total flux seen by the detectors in this condition is much larger than the flux they see during normal observation, leading to changes in the bolometer operating points. While we have allowed for these effects, the fit of the calibration model to the data is still preliminary for $\nu > 50$ cm^{-1}. As a result, quantities that depend on absolute gains, such as the luminosity of the Galaxy, or on the ratio of gains at widely separated frequencies, such as interstellar dust temperatures, have larger uncertainties than we will ultimately achieve. Line frequencies and line to continuum ratios should not be affected, and line fluxes at long wavelengths ($\lambda > 250$ μm) are calibrated to 3%.

The FIRAS data have been accumulated into pixels on the sky, using the quadrilateralized spherical cube of Chan & O'Neill (1975). The cube faces are centered on the coordinate axes of the J2000 ecliptic coordinate system. A total of 6144 equal-area quadrilateral pixels cover the sky, and the map presented here has 4022 pixels covered, including 72% of the Galactic plane region with $|b| < 14°$.

3. RESULTS

3.1. *Mean Spectrum*

While the dust, [C II], and [N II] emissions are strong enough to see in individual pixels, the fainter features of the Galactic spectrum require the co-addition of large numbers of pixels to provide adequate signal-to-noise ratios. In order to maximize the sensitivity, a weighted mean spectrum is constructed by a least-squares fit. The basic assumptions were presented by Wright et al. (1990): the Galaxy spectrum as a function of position and frequency is assumed to factor into a function of position times a function of frequency:

$$I_G(l, b, \nu) = G(l, b)g(\nu) . \quad (1)$$

This is obviously an approximation because it ignores spatial variations in the shape of the spectrum, but it is suitable for obtaining large-scale averages and enhancing the detectability of faint features. Mathematically this procedure corresponds to using a matched spatial filter to measure the galaxy spectrum, where the filter is matched to the dust continuum. The map of the galaxy $G(l, b)$ is obtained taking an estimate for the galaxy spectrum $g_0(\nu)$ and fitting the following function to the spectrum at each pixel:

$$I(l, b, \nu) = B_\nu[T_0 + \Delta T(l, b)] + G(l, b)g_0(\nu) , \quad (2)$$

where $B_\nu(T)$ is the Planck function. The ΔT term represents the FIRAS measurement of the anisotropy of the cosmic microwave background and is well represented by a dipole pattern on the sky (Cheng et al. 1990). T_0 is the temperature of the cosmic microwave background, taken to be 2.735 K (Mather et al. 1990). Note that $g_0(\nu)$ is used only to find the spatial function $G(l, b)$. We have used a simple functional form for $g_0(\nu)$ based on the first two months of FIRAS data:

$$g_0(\nu) \equiv 0.0002(\nu/30\ cm^{-1})^{1.5}B_\nu(T_d) , \quad (3)$$

where the dust temperature $T_d = 21.75$ K. This form for $g_0(\nu)$ was chosen because the simpler functions with dust emissivities varying like ν^1 or ν^2 gave significantly poorer fits for $1 < \nu < 50$ cm^{-1}. The arbitrary scaling factor in $g_0(\nu)$ defines the levels on the map $G(l, b)$ which is shown in Figure 1. The choice of the "0.0002" factor in $g(\nu)$ brings the typical level of $G(l, b)$ close to unity. [In § 3.3 we estimate that $G(l, b) = 1$ corresponds to $I(\mathrm{bol}) = (5.9 \pm 2) \times 10^{-3}$ ergs cm^{-2} s^{-1} sr^{-1}.] Using the $G(l, b)$ derived by fitting the map, the mean spectrum of the galaxy and the spectrum of the dipole are found by fitting all the data at a given frequency to the form

$$I(l, b, \nu) = I_0(\nu) + \cos\theta\, d(\nu) + G(l, b)g(\nu) , \quad (4)$$

where θ is the angle between (l, b) and the hot pole of the dipole anisotropy (265° ± 2°, 48° ± 2°) (Smoot et al 1991). The dipole spectrum $d(\nu)$ obtained in this fit is equivalent to the spectrum

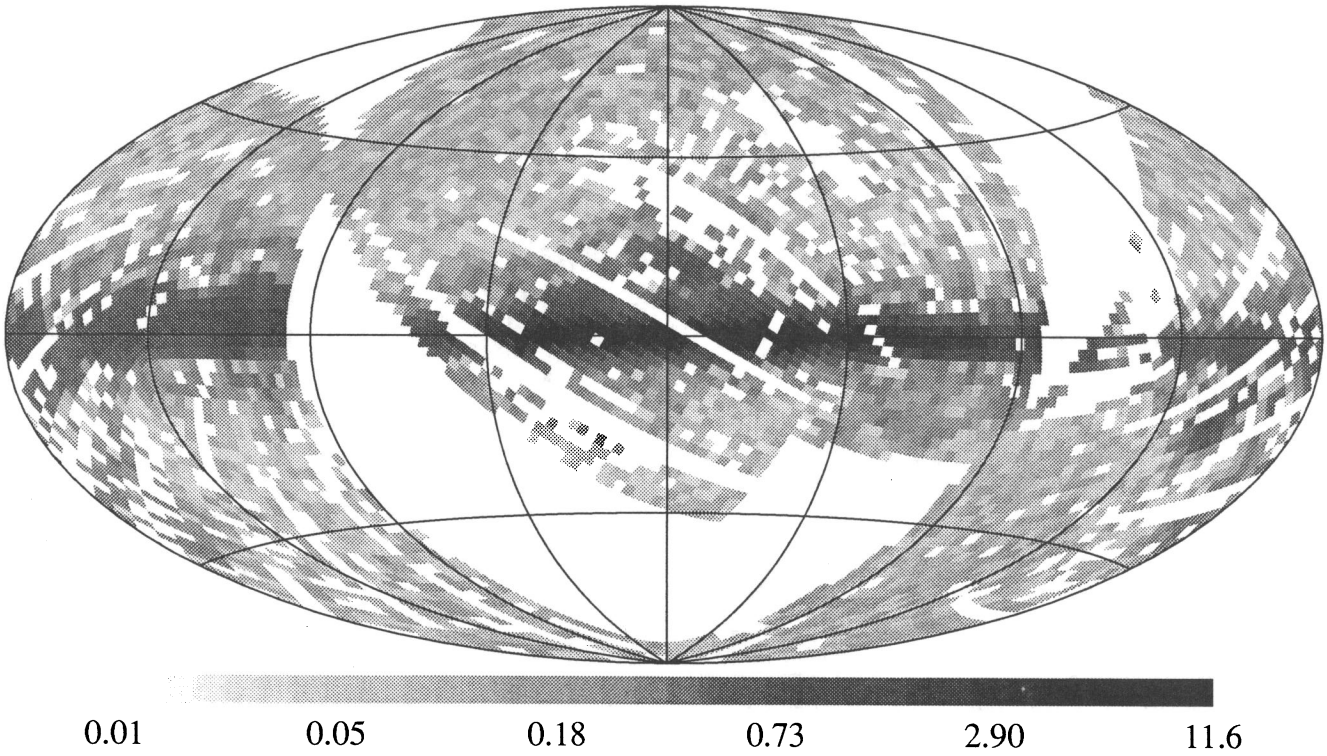

FIG. 1.—Gray-scale representation of the FIRAS dust map, $G(l, b)$ (see eqs. 2 and 3)

presented by Cheng et al. (1990). The average galaxy spectrum $g(\nu)$ is shown in Figure 2. Any all-sky map can be analyzed in this way, and the maps from the differential microwave radiometers (DMR) instrument on COBE have been used to generate the three data points shown as closed circles at 1.03, 1.77, and 3 cm^{-1}. We have assumed a 20% error for the DMR points, which is much larger than the actual noise, to allow for possible systematic effects caused by different beam shapes and sidelobes. Note that the FIRAS data from 20–23 cm^{-1} are very poorly calibrated since they are at the edge of the passband of the dichroic filter used to separate the high- and low-frequency channels; these points and the noisy data from 50–90 cm^{-1} were not used to find $G(l, b)$.

We have tried several different forms of analytic fits to the continuous part of the mean galactic spectrum $g(\nu)$. The weights used in these fits are based on assumed values of σ

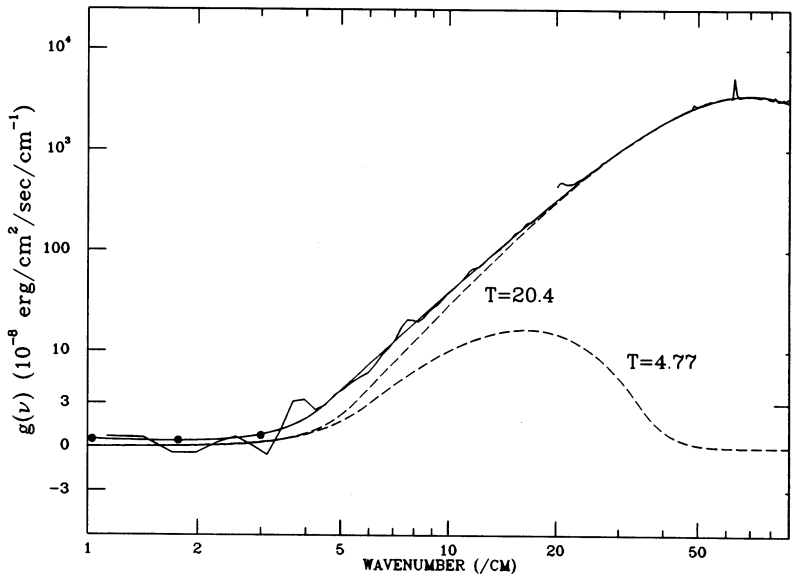

FIG. 2.—Average galaxy spectrum. Note that the scale changes from logarithmic to linear at low intensities [$g(\nu) < 3$] in order to accommodate negative values. Here $g(\nu)$ is the mean sky spectrum where $G(l, b) = 1$. The three low-frequency points are from the DMR. The smooth curve is a two-temperature dust plus synchrotron model (eq. 5). Dashed curves show the individual dust components with ν^2 power-law emissivities.

equal to the larger of 3×10^{-8} ergs cm^{-2} s^{-1} cm^{1} sr^{-1} or a percentage of the flux ranging from 3% for $\nu < 20$ cm^{-1} to 31% at 80 cm^{-1}. The actual scatter of the data is much less than this. The most successful fit uses the sum of two components with emissivities going like ν^2 and different temperatures. In order to fit the rise seen at low frequencies by the DMR, we have added a synchrotron term as well. The spectral index of this low-frequency component cannot be determined with *COBE* data alone, so we have assumed an index of $I_\nu \propto \nu^{-0.75}$. The resulting analytic fit to the continuous part of the galaxy spectrum is

$$g(\nu) \approx 0.00022(\nu/30 \text{ cm}^{-1})^2 \times [B_\nu(20.4) + 6.7B_\nu(4.77)] + S(\nu) , \quad (5)$$

where the synchrotron term $S(\nu)$ corresponds to a Rayleigh-Jeans brightness temperature of 0.6 mK at 1 cm^{-1}. This fit is shown in Figure 2 as the smooth solid curve, and the dust components of the fit are shown as dashed curves. The spectrum of the dust varies from place to place on the sky, and this average spectrum will change as sky coverage increases from the 65% analyzed here to the 98% actually covered by FIRAS. We consider the "cold dust" above to be a convenient way to express the long-wavelength excess over a ν^2 emissivity model. This excess suggests but does not prove the existence of some grains that are efficient long-wave emitters, such as conducting needles or fractal dust grains (Wright 1987). The cooler fitted component accounts for only 0.11% of the total dust luminosity.

The data can also be modeled by a single temperature dust with a power law emissivity. The result for the data in this paper is

$$g(\nu) \approx 0.00016(\nu/30 \text{ cm}^{-1})^{1.65}B_\nu(23.3) + S(\nu) , \quad (6)$$

where the synchrotron term gives 0.64 mK at 1 cm^{-1}. The difference between this fit and $g_0(\nu)$ is due to the inclusion of more data including the Galactic center which contains warmer dust than the regions scanned by FIRAS in its first two months of operation. The χ^2 of this fit is twice as high as that of the two-temperature model, with 321 data points. If statistical noise were the only concern, this difference in χ^2 would decide in favor of the two-temperature model presented earlier, but the difference between this model and the two-temperature model is a small, slowly varying function of frequency. The maximum difference between the two models is -12% at 5 cm^{-1} where the signal is weak, and 9% at 90 cm^{-1} where the calibration is likely to be poor. The systematic calibration uncertainties in the high-frequency channel could produce gain errors that are small, slowly changing functions of frequency, so this approximation to $g(\nu)$ cannot be ruled out.

Other groups have also seen excess low-frequency emission (over a ν^2 emissivity law) from Galactic dust. Our spectrum $g(\nu)$ has a smaller low-frequency excess than the Page, Cheng, & Meyer (1990) spectrum or the Meinhold & Lubin (1991) spectrum. The ratio of flux at 5.6 cm^{-1} to the continuum flux at 63.4 cm^{-1} in $g(\nu)$ is 0.65 times that given by Page et al. We have convolved the *IRAS* 100 μm map with a 7° beam, and then fitted it to Equation 4, and obtain 70 ± 14 MJy sr^{-1} at unit level of the map [$G(l, b) = 1$]. (Note that this *IRAS* value has not been corrected for the "AC-DC" effects seen by Hauser et al. [1989], but the appropriate correction is not easy to determine: we assume a 20% uncertainty.) The 3 cm^{-1} DMR map gives 104 ± 21 μK at unit level of the map. Thus we obtain a ratio of 1.5 ± 0.5 μK/(MJy sr^{-1}) compared to 17–18 μK/(MJy sr^{-1}) found by Meinhold and Lubin. However, the shape of the dust spectrum in the FIRAS data does change with position, and a detailed discussion of the dust spectrum should wait until the entire FIRAS data set can be analyzed and compared with the diffuse infrared background experiment (DIRBE) data.

The average spectrum $g(\nu)$ has been searched for lines by fitting a power-law continuum plus the line to a section of the spectrum that is either 1 cm^{-1} wide for the low-frequency ($\nu < 20$ cm^{-1}) long-scan data or 4 cm^{-1} wide for the short-scan data. The line shape used in the fit is the instrumental profile which is determined by the apodization function. Two examples of these fits are shown in Figure 3. The results of the line fits are shown in Table 1. A footnoted frequency indicates that no significant line flux was seen at this frequency. For other lines, the frequency given is the best fit to the FIRAS line. We assume that the different phases of the ISM which contribute to the different lines in the average spectrum are sufficiently well mixed that their average velocities agree to better than our accuracy of 100 km s^{-1}, and have not made any corrections for Galactic kinematics. The line fluxes presented in the table are the average of the fluxes observed in the LF and SS modes for frequencies less than 20 cm^{-1}, while for higher frequencies only the SS mode data are used. Because only a small number of data points go into each line fit, and the apodization causes point-to-point correlations, the distribution of errors from this fit is not Gaussian. The flux errors given are for a 68% confidence interval, but errors 3 times larger than this occur 3% of the time. We have examined the entire spectrum for unknown lines and saw only one candidate outside of the ± 3 "sigma" 97% confidence interval. This candidate had a rather low line flux, indicating that it was a coincidental pattern of noise that looked like a line, rather than a true line. The sensitivity of this line search is variable, being least sensitive at the high-frequency end of the spectrum or close to the strong lines.

3.2. [N II] *Lines*

We have observed a line at 205.3 μm which we identify as [N II]. This line is 1/10 as strong as the [C II] line and is the second strongest line in the 1–80 cm^{-1} frequency range. Our

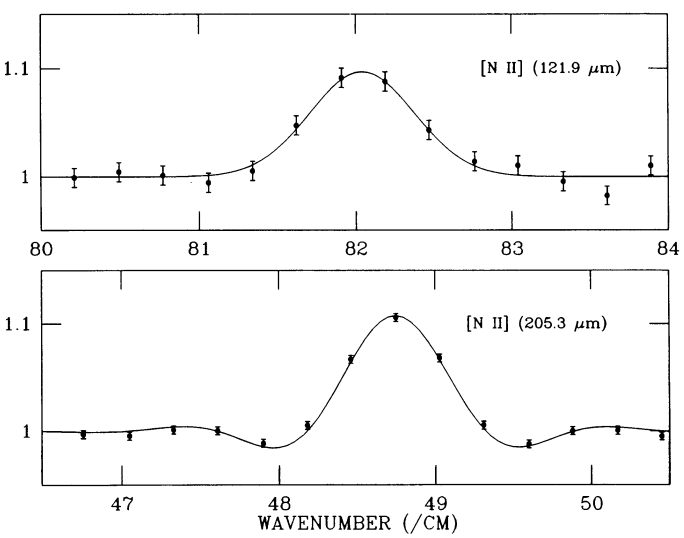

FIG. 3.—The [N II] lines in the mean spectrum. Fluxes have been normalized to a power-law continuum.

observations give a frequency of 48.700 cm^{-1} in the SS mode, and 48.729 cm^{-1} in the LF mode. The special long-scan data with offset data collection are limited but give 48.727 $\pm$ 0.008 cm^{-1} for the [N II] line when we assume 63.395 cm^{-1} for the [C II] line. The unweighted average frequency and 1 σ uncertainty is 48.719 $\pm$ 0.009 cm^{-1} for the [N II] line, or $\lambda = 205.26 \pm 0.04$ μm. Mendoza's 1983 review gives Edlén's (1972) value of 48.7 cm^{-1} for the predicted frequency of this line, but no laboratory measurements of its wavelength have been made. The predicted wavenumber for the 122 μm line was in error by only 0.07% so the coincidence of the predicted and measured frequencies is a strong indication that the line we observe should be identified with [N II]. We find that the 205 μm line is more concentrated in the Galactic plane than either the dust continuum or the [C II] line.

The ionization potential of N is 14.5 eV, so nitrogen is expected to be neutral in H I regions, but will be totally ionized within H II regions. Rubin (1985) has computed the expected strengths of many lines including the [N II] lines. The ratio of the 122 μm line flux to the 205 μm flux for [N II] is predicted to be 3:1 in low-density ($n_e = 100$ cm^{-3}) H II regions excited by stars with $T_{\rm eff} = 33{,}000$ K, and is not sensitive to $T_{\rm eff}$. For high-density regions the ratio saturates at 10:1. The ratio of the [C II] line to the 205 μm line ranges from 4:1 to 7:1 in Rubin's models. Thus our observed ratio of 10:1 for the 158 μm flux to the 205 μm flux could be explained by assuming that one-half of the [C II] flux comes from H I regions that produce no [N II], and half comes from H II regions.

We have seen the 122 μm line of [N II] as well. Even though the line flux is strong, the optical efficiency of FIRAS at this frequency is low, so this line is not strong enough to map. The measured line appears broader than the lines seen at lower frequencies, indicating that beam divergence in the FIRAS optics is reducing the modulation contrast of the fringes as the optical path length increases. Allowing the instrumental line width to be a free parameter, the fitted line strength of the 122 μm line is 1.6 $\pm$ 0.2 times the strength of the 205.3 μm line in the average Galactic spectrum (see Table 1). If the line width is constrained to the width observed for the [C II] line, then the flux ratio is only 1:1. Both of these ratios are considerably less than the lower end of the line ratios in Rubin's (1985) H II region models, but higher than the ratio of 0.7:1 that would obtain in the low-density limit where almost all nitrogen ions are in the ground fine structure state.

At 5000 K electron temperature, the collisional de-excitation of the $^3P_1$ upper level of the 205 μm line equals the radiative decay rate for an electron density of $n_e = 130$ cm^{-3}. To obtain the line ratio seen by FIRAS, most of the [N II] emission must come from a medium with $n_e \ll 100$ cm^{-3}. Ratios of 122:205 flux from 1:1 to 1.6:1 are obtained for uniform density models with n_e between 10 and 35 cm^{-3}. Inhomogeneous models where some of the [N II] emission comes from H II regions giving a ratio of 3:1, while the rest of the [N II] emission comes from low-density regions, such as the warm ionized medium (WIM) proposed by McKee & Ostriker (1977) with $n_e = 0.2$ cm^{-3}, require that 60% of the 205 μm emission comes from the low-density regions for a 1.6:1 line ratio. Then the 40% of the 205 μm emission that comes from H II regions will be confined to the Galactic plane, leading to the observed enhanced concentration in the plane of the [N II] relative to the dust or [C II].

Reynolds (1989) gives an electron density distribution that implies a column density of 10^{20} toward the Galactic pole,

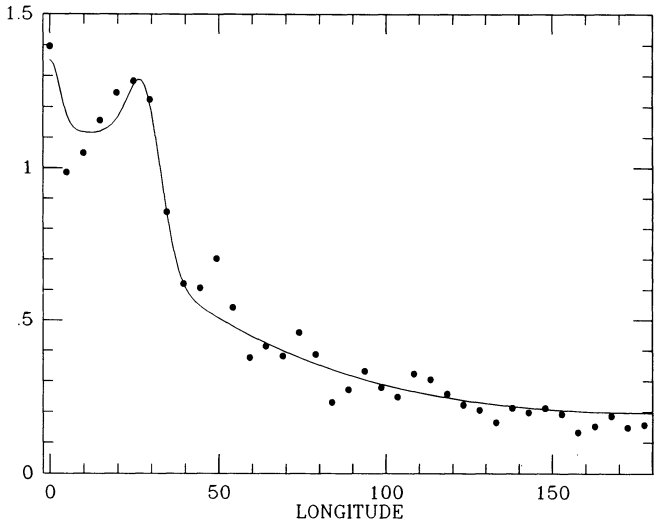

FIG. 4.—Longitude profiles of the Galactic dust constructed by integrating $G(l, b)$ over $|b| < 14°$. Solid circles are continuum points, and the curve is a model for the continuum.

which implies a column density of N^+ of 10^{16} if all of the cosmic abundance of nitrogen is singly ionized wherever the hydrogen is ionized. If $n_e = 0.3$ and $T_e = 10^4$ in the WIM clouds, then this column density of N^+ will produce a 205 μm flux of 8×10^{-8} ergs cm^{-2} sr^{-1} s^{-1}. Since the Galactic poles correspond roughly to $G(l, b) = 0.05$, this agrees quite well with a linear scaling of the flux in Table 1. Thus the strength of the 205 μm line is consistent with the picture of a WIM having $n_e = 0.3$, a filling factor of 0.08 (Kulkarni & Heiles 1986), and a scale height of 1500 pc.

3.3. [C II] *and Total Luminosity*

It is not possible to determine uniquely the total luminosity of the Galaxy from a viewpoint within the disk. Therefore we have made a model fit to the longitude profile in order to determine the total luminosity. Since the map used in this work does not cover all of the sky, the intensities at $(-l, b)$, $(-l, -b)$, and $(l, -b)$ are averaged with the intensity at (l, b) to get a more fully covered map. The basic FIRAS pixels are 2°.6 squares, which are smaller than the beam. We have averaged the values into boxes 5° in longitude by 0.1 in sin b to construct the profiles. After folding in longitude and latitude and using the larger boxes we do have complete coverage. Since the map function $G(l, b)$ is defined to be dimensionless, the longitude profile based on integrating the map over latitude has the dimensions of radians. The dust profile is shown in Figure 4 as the solid circles. This profile is the integral of $G(l, b)$ from $-14°$ to $+14°$ in Galactic latitude b. Restricting the range of the b-integral reduces the noise while including most of the flux.

The solid curve in Figure 4 shows the model fit to the dust profile. The model we use for this latitude integral of $G(l, b)$ has three components: a central Gaussian, an exponential disk, and a molecular ring with a Gaussian radial profile. The emissivity in this model depends only on r, the radius of a point in the disk expressed in units of R_0, the distance from the Sun to the Galactic center:

$$j(r) = 1.79 \exp(-204r^2) + 0.5 \exp(-r/1.03) + 0.9 \exp[-112(r - 0.501)^2] . \quad (7)$$

Integrating the total luminosity of the model gives a total of 3.9 sr for the appropriate integral of the map. This is a rather large value because the best-fit scale length for the exponential disk in the model is $1.03R_0$. Confining the integration of the model to the region inside the solar circle ($r < 1$) gives 1.35 sr for the factor to use when computing the luminosity within the solar circle. If the Galaxy were spherical, then the appropriate integral for the luminosity within the solar circle is $\int G(l, b) \cos b \cos l \, d\Omega = 1.41$ sr, so the luminosity is not critically dependent on the assumptions used in the disk model fit. The unweighted integral of the map over 4π gives 3.8 sr, which is useful for computing the mean intensity. Since the peak of the map at the Galactic center is 12, the effective solid angle of the map is really 0.3 sr.

The measured spectrum does not cover the entire far-infrared region. We can make a fairly reliable estimate of the line to continuum ratio at the [C II] line frequency, even though the calibration at frequencies higher than 50 cm^{-1} is uncertain. We get $I(\text{line})/\nu I_\nu(\text{cont}) = 0.0082$. The spectra of three Galactic regions given by Pajot et al. (1986) and the 160 μm photometry of four normal Virgo cluster spirals by Stark et al. (1989) can be used to estimate that the ratio of continuum flux at the [C II] line to the bolometric flux is $\nu I_\nu(\text{cont})/I(\text{bol}) = 0.36 \pm 0.05$, so the ratio of the [C II] line to the total flux is $I(C^+)/I(\text{bol}) = 0.003$, where we have integrated our spectrum combined with Pajot et al. and Stark et al. spectra from 10 to 1000 μm to define I(bol). The value of the continuum at the [C II] line is 112 MJy sr^{-1} at unit level on the map $G(l, b)$, giving an extrapolated bolometric intensity of 5.9×10^{-3} ergs cm^{-2} s^{-1} sr^{-1}. These fluxes could be in error by as much as 30%, because both the FIRAS calibration and the extrapolation to bolometric intensity are uncertain. The resultant total far-infrared luminosity of the Galaxy is

$$L = 4\pi R_0^2(1.35 \text{ sr})(5.9 \times 10^{-3} \text{ergs cm}^{-2} \text{ s}^{-1} \text{ sr}^{-1}) \quad (8)$$

or $L = (1.8 \pm 0.6) \times 10^{10} \, L_\odot$. Our uncertainty in this value includes 20% due to the 5% uncertainty in our calibrator temperature at 20 K, 10% due to uncertainties in the map folding and model fitting procedure, and 25% due to uncertainties in the extrapolation to I(bol). Our luminosiy is about 25% larger than the earlier results of Hauser et al (1984) and Gispert et al. (1982) after scaling their figures to $R_0 = 8.5$ pc, but this difference is smaller than the errors. Sodroski et al. (1989) give far-IR luminosities that are 30% smaller than Gispert et al. and thus depart further from the FIRAS estimate, but they do not include the mid-infrared emission from transiently heated grains, which they estimate would increase the infrared luminosity by 30%–50%.

While gradients in the ratios of lines to dust are certainly present, we estimate the line luminosities of the Galaxy by a simple linear scaling law:

$$L(\text{line}) = 4\pi R_0^2[(1.35 \text{ sr}) I(\text{line})]$$
$$= 3 \times 10^4 \, L_\odot [I(\text{line})/10^{-8} \text{ ergs cm}^{-2} \text{ s}^{-1} \text{ sr}^{-1}] , \quad (9)$$

where $[I(\text{line})/10^{-8}$ ergs cm^{-2} s^{-1} $sr^{-1}]$ is the number tabulated in Table 1. These total luminosities are also given in Table 1.

3.4. *Galactic Gradients*

Maps have been made of the [C II] and [N II] line fluxes by fitting line profiles to the spectrum in each pixel and are shown in Figures 5 and 6, respectively. These maps have been binned

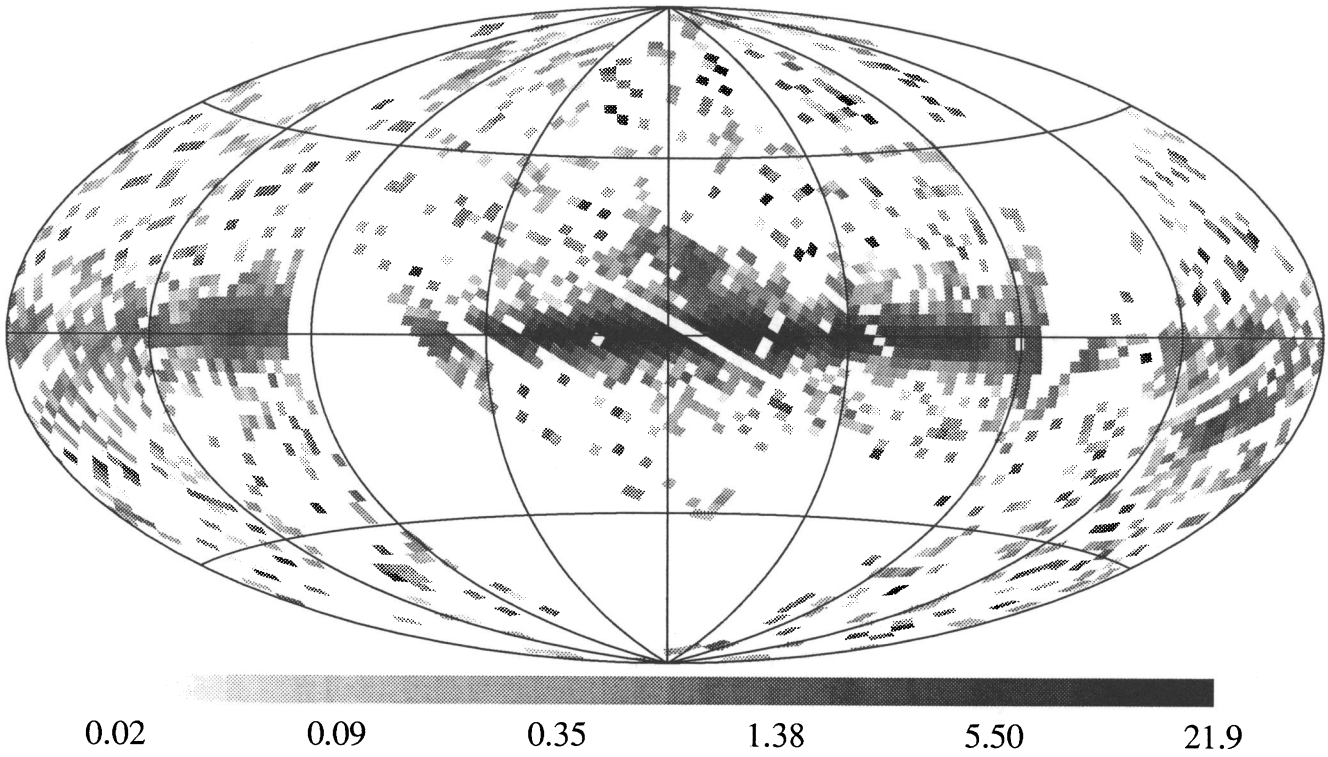

FIG. 5.—Gray-scale representation of [C II] line flux at 158 μm. Units on the scale bar are 10^{-5} ergs cm^{-2} s^{-1} sr^{-1}

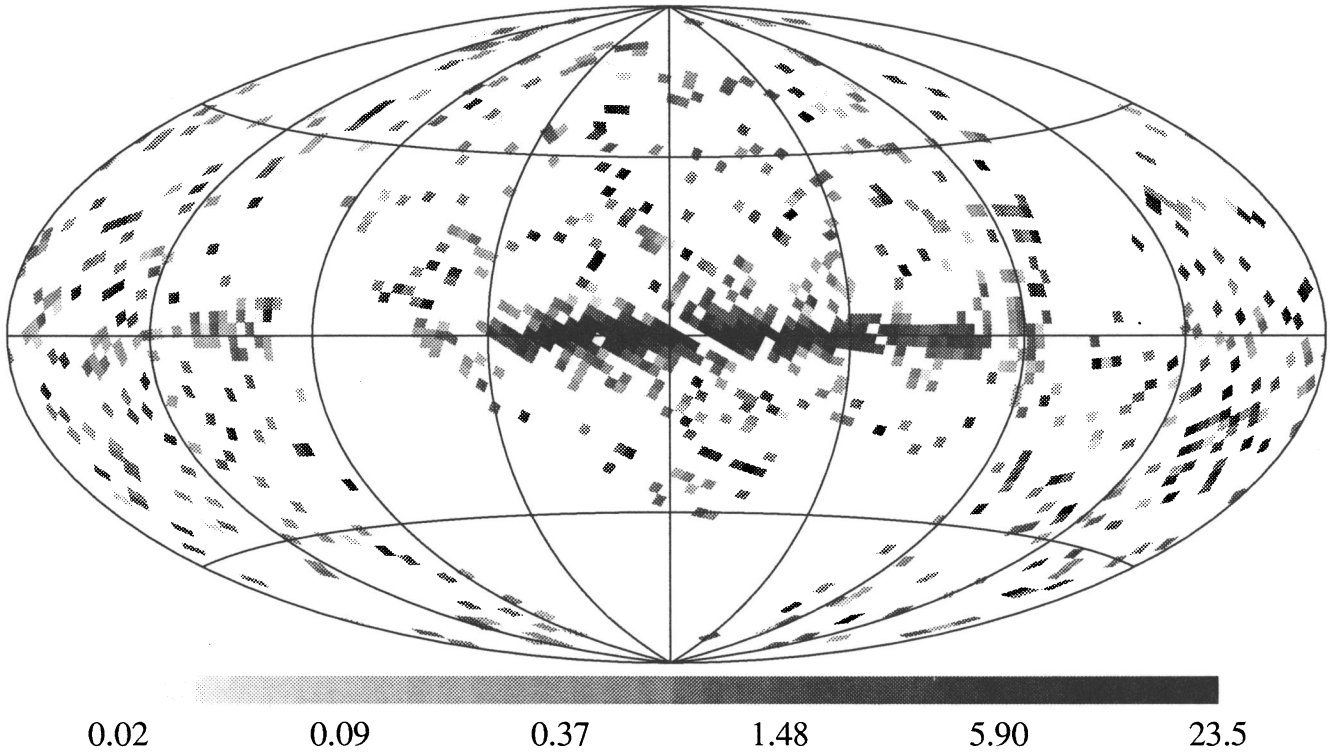

FIG. 6.—Gray-scale representation of [N II] line flux at 205.3 μm. Units on the scale bar are 10^{-6} ergs cm^{-2} s^{-1} sr^{-1}

and folded like the dust map to give the correlation plots shown in Figures 7 and 8. Figure 7 shows the dependence of the [C II] line strength on the dust continuum as measured by $G(l, b)$. The only major difference between the dust and [C II] distribution occurs at the Galactic center, which is a peak in the dust but a plateau in the [C II]. This may indicate differences in dust temperature, in photoelectric efficiency of the grains, in the color of the ambient interstellar radiation field due to stellar population or reddening, or the saturation of the [C II] cooling rate when the level populations are in equilibrium with dense warm gas. Figure 8 shows the dependence of the [N II] line flux on the [C II] line flux. In bright regions of the sky the two lines are roughly proportional to each other, but there appears to be a threshold [C II] brightness before the [N II] starts to rise. All of the points near the origin are from high-latitude regions, so this apparent threshold is probably caused by a relative lack of [N II] emission from high-latitude cirrus.

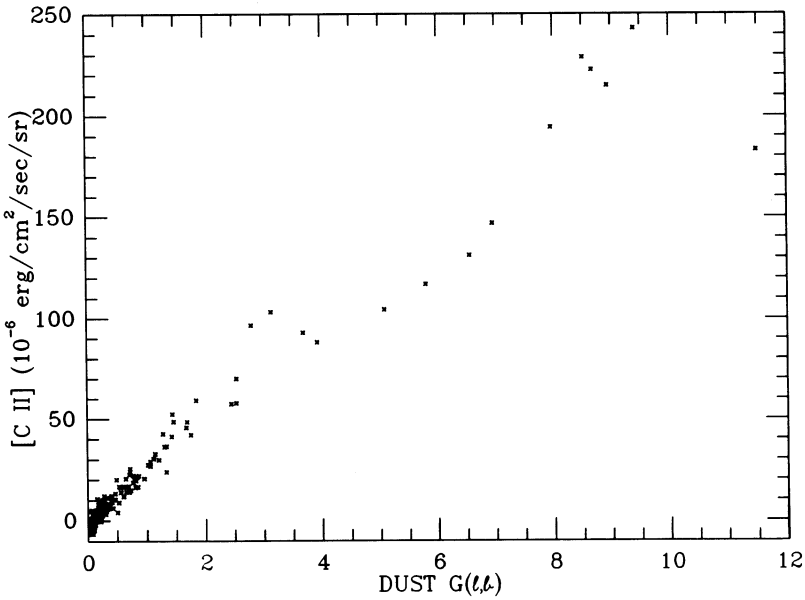

FIG. 7.—Strength of the [C II] line vs. the dust continuum mapped in Fig. 1. The original map was folded and binned to make this plot.

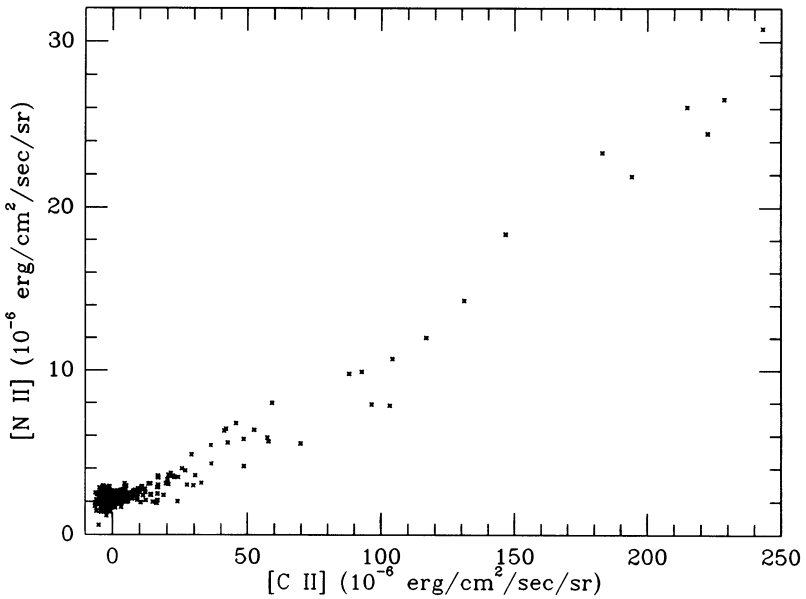

FIG. 8.—Strength of the 204 μm [N II] line vs. the [C II] line, after folding and binning

4. DISCUSSION

The dust and gas emissions coming from the Milky Way are not unusual when compared to the external galaxies observed by Stacey et al. (1991). The [C II] to bolometric flux ratio is 0.3%, similar to that seen in external galaxies (Crawford et al 1985, Stacey et al. 1991). The $I(C^+):I(CO\ J = 1–0)$ ratio is poorly determined from FIRAS data because of the weakness (in ergs, not K km s^{-1}) of the $J = 1–0$ CO line. However, the ratio from FIRAS is consistent with the standard correlation of $I(C^+):I(CO\ J = 1–0) = 4400$ (Wolfire, Hollenbach, & Tielens 1989). Furthermore, the CO 1–0 line flux found using FIRAS is consistent with the CO map presented by Dame et al. (1987) within the uncertainty caused by the FIRAS beam being larger than the latitude range covered by the ground-based survey.

The ratios of the CO lines seen in the average galaxy spectrum indicate the presence of several temperatures, as expected. Assuming optically thin emission from CO in local thermodynamic equilibrium (LTE), we can fit the line ratios reasonably well using a two-temperature model, with 88% of the CO at 5 K and 12% at 19 K. Of course, in reality, there is some smooth distribution of temperatures, and the assumption of LTE level populations in optically thin CO is unrealistic. But with only four well-detected CO lines, we have only three ratios and can only determine three parameters of the temperature distribution. For this simple model, the column density of CO at unit level on the map $G(l, b)$ is 3×10^{15} cm^{-2}. The 1–0 CO flux predicted from these fitted temperatures is 0.5×10^{-8} ergs cm^{-2} s^{-1} sr^{-1}, compared to the observed $(0.6 \pm 0.7) \times 10^{-8}$ ergs cm^{-2} s^{-1} sr^{-1}. Dividing the [C II] flux by the canonical ratio of 4400:1 predicts 0.4×10^{-8} ergs cm^{-2} s^{-1} sr^{-1} for the 1–0 CO line flux.

The ratio of fluxes in the [C I] lines is $I(370\ \mu m)/I(609\ \mu m) = 2$. For optically thin emission this implies one relation between the temperature and density of the emitting gas, such that $T = 25$ K for infinite density, $T = 50$ K for a density of 600 cm^{-3}, or the density is 130 cm^{-3} for high T, where we have used the collision cross sections given by Zmuidzinas et al (1988). They found that the antenna temperature of the 370 μm [C I] line is typically 12% of that for the 2–1 CO line, while the fluxes found by FIRAS give 10% for the ratio of K km s^{-1} for these lines. This good agreement suggests that the bulk of total Galactic [C I] and CO emission comes from dense molecular clouds similar to those observed by Zmuidzinas et al.

The upper limit on the [O I] line at 145.5 μm shows that most of the neutral interstellar gas is too cold to excite the upper level, which is 327 K above the ground state. Even in hotter regions this line is not strong (Stacey et al. 1983a). The PDR (photodissociation region) models of Tielens & Hollenbach (1985) predict that this line will be less than our measured limit if either the density of the cold molecular cloud (n_0) that is being ionized and dissociated is low, or the UV flux is low. In order to obtain a low enough 145 μm to 158 μm ratio, the FIRAS data require $n_0 < 10^{3.4}$ cm^{-3}. The ratio of the [C I] lines in the FIRAS data also requires a low $n_0 \approx 10^{3.4}$ in the Tielens and Hollenbach PDR models. Thus the Tielens and Hollenbach PDR model with $n_0 \approx 2500$ cm^{-3} is consistent with the FIRAS limit on the 145 μm [O I] line, the ratio of the [C I] lines, and the ratio of the 158 μm [C II] line to the [C I] lines. Hollenbach, Takahashi, & Tielens (1991) provide a grid of PDR models with lower densities and lower incident UV fluxes than the Tielens and Hollenbach standard model, and many of these combinations of UV flux and density can match the FIRAS line ratios.

We have made the first detection of the 205 μm line of [N II], and it is the second strongest line in the 1–80 cm^{-1} frequency range. The ratio of the 122 μm line to the 205 μm line is only 1.6:1, which implies that about one-half of the [N II] emission comes from ionized gas with $n_e \ll 100$ cm^{-3}, consistent with the WIM proposed by McKee & Ostriker (1977), Sodroski et al. (1989) estimate that only 8%–10% of the far-infrared luminosity of the Galaxy comes from extended low-density H II regions. This small fraction does not provide enough [N II] flux to explain the FIRAS data. The Rubin (1985) model with $T_{\rm eff} = 33{,}000$ K, Kurucz abundances and $n_e = 100$ cm^{-3} gives the highest ratio of [N II] flux per Lyman continuum photon among all Rubin's models. Increasing the predicted 205.3 μm flux of this model by a factor of $(1 + n_e/n_{\rm crit}) = 1.7$ (to allow for

the collisional de-excitation that equals the radiative decay at $n_{crit} = 146$ cm^{-3} for the $T_e = 6563$ K of the model) gives a predicted line flux of $0.0033 L_{FIR}$/IRE for much lower density regions, where IRE is the infrared excess for the H II regions. Sodorski et al. give an average IRE = 2.5, so the expected fraction of the far-infrared luminosity in the 205 μm line is 0.012%. The observed value is 0.03%, and therefore either the nitrogen abundance is enhanced by a factor of 2.5, or there is additional ionized gas not recognized by Sodroski et al. The WIM phase of the McKee and Ostriker model could provide this extra plasma. The low electron density in the WIM gives it a low emission measure, so it does not radiate much of the 5 GHz radiation used by Sodroski et al. to locate ionized gas. Since the WIM is intimately associated with the WNM which provides the H I flux in the McKee and Ostriker model, the far-infrared flux from the WIM would be assigned to the H I component by the Sodroski et al. analysis. Sodroski et al. find that the H I component emits 60%–75% of the far-infrared luminosity. About one-quarter of this flux must come from low-density regions where nitrogen is ionized in order to explain the observed [N II] flux without an enhanced nitrogen abundance.

Several molecular lines of interest to submillimeter astronomy were searched for and not seen. In particular, low-lying molecular oxygen and water lines are weaker than the nearby CO lines. Thus, the filling factor of the dense phases of the interstellar medium that radiate water and molecular oxygen lines must be small. The [S I] line at 129.7 μm was also not seen.

Finally, we want to emphasize the preliminary nature of these results. Expected progress in the FIRAS data processing will certainly allow refinements of these results in the future. The calibration of the high-frequency channel will be improved. Improved algorithms for removing cosmic-ray glitches from the low-frequency channel data should give lower noise, which may allow FIRAS to measure the dust emission to longer wavelengths and to map weaker lines. Shorter wavelength data from the DIRBE experiment will be added to the analysis. We have analyzed only half of the total data and two-thirds of the total sky coverage in this paper. Adding the rest of the sky coverage will certainly change the mean spectrum, since spatial variations of the spectral shape have been seen.

This work was supported by the NASA Astrophysics Division through the *COBE* project. It is a pleasure to acknowledge the vital contributions of the GSFC management and engineering staff, the hundreds of contractors, and the launch crew, who made this challenging mission possible. Conversations with E. Dwek are especially appreciated.

REFERENCES

Boreiko, R. T., Betz, A. L., & Zmuidzinas, J. 1988, ApJ, 325, L46
Chan, F. K., & O'Neill, E. M. 1975, Feasibility Study of a Quadrilateralized Spherical Cube Earth Data Base (EPRF Technical Report 2-75) (NTIS Report A0-A010232) (Computer Sciences Corp.)
Cheng, E., Mather, J., Shafer, R., Meyer, S., Weiss, R., Wright, E., Eplee, R., Isaacman, R., & Smoot, G. 1990, Bull. Am. Phys. Soc., 35, 971
Cox, D. P., & Reynolds, R. J. 1987, ARA&A, 25, 303
Crawford, M. K., Genzel, R., Townes, C. H., & Watson, D. M. 1985, ApJ, 291, 755
Dalgarno, A., & McCray, R. A. 1972, ARA&A, 10, 375
Dame, T. M., et al. 1987, ApJ, 322, 706
Edlén, B. 1972, Solar Phys., 24, 356
Field, G. B., Goldsmith, D. W., & Habing, H. J. 1969, ApJ, 155, L149
Genzel, R. 1991, Proc. Conf. on Molecular Clouds, March 1990, Manchester, UK, ed. R. James & T. Millar (MPE Preprint 181)
Genzel, R., Harris, A. I., & Stutzki, J. 1989, in Infrared Spectroscopy in Astronomy, ed. B. H. Kaldeich (ESA SP-290) (Noordwijk: ESA Publication Div.)
Gispert, R., Puget, J. L., & Serra, G. 1982, A&A, 106, 293
Hauser, M. G., et al. 1984, ApJ, 285, 74
Hauser, M. G., Kelsall, T., Moseley, S. H., Silverberg, R. F., Murdock, T. L., & Wright, E. L. 1989, BAAS, 21, 1219
Hauser, M. G., Kelsall, T., Moseley, S. H., Jr., Silverberg, R. F., Murdock, T., Toller, G., Spiesman, W., & Weiland, J. 1991, in After the First Three Minutes, ed. S. S. Holt, C. L. Bennett, & V. Trimble (AIP CP-222) (New York: American Institute of Physics), 161
Hoffman, W. F., & Frederick, C. L. 1969, ApJ, 155, L9
Hollenbach, D. J., Takahashi, T., & Tielens, A. G. G. M. 1991, ApJ, 377, 192
Jaffe, D. T., Harris, A. I., Silber, M., Genzel, R., & Betz, A. L. 1985, ApJ, 290, L59
Kulkarni, S. R., & Heiles, C. 1986, in Interstellar Processes, ed. D. J. Hollenbach & H. A. Thronson (Dordrecht: Reidel), 87
Lockman, F. J. 1976, ApJ, 209, 429
Low, F. J., Kurtz, R. F., Poteet, W. M., & Nishimura, T. 1977, ApJ, 214, L115
Mather, J. C., et al. 1990, ApJ, 354, L37
McKee, C., & Ostriker, J. P. 1977, ApJ, 218, 148
Meinhold, P., & Lubin, P. 1991, ApJ, 370, L11
Mendoza, C. 1983, in Proc. IAU Symp. 103, Planetary Nebulae, ed. D. R. Flower (Dordrecht: Reidel), 143
Page, L. A., Cheng, E. S., & Meyer, S. S. 1990, ApJ, 355, L1
Pajot, F., Boisse, P., Gispert, R., Lamarre, J. M., Puget, J.-L., & Serra, G. 1986, A&A, 157, 393
Phillips, T. G., Huggins, P. J., Kuiper, T. B. H., & Miller, R. E. 1980, ApJ, 238, L103
Reynolds, R. J. 1984, ApJ, 282, 191
———. 1989, ApJ, 339, L29
Reynolds, R. J., Roesler, F. L., & Scherb, F. 1977, ApJ, 211, 115
Rubin, R. H. 1985, ApJS, 57, 349
Rubin, R. H., Hass, M. R., Erickson, E. F., Simpson, J. P., & Colgan, S. W. J. 1989, BAAS, 21, 1213.
Russell, R. W., Melnick, G., Gull, G. E., & Harwit, M. 1980, ApJ, 240, L99
Smoot, G. F., et al. 1991, ApJ, 371, L1
Sodroski, T. J., Dwek, E., Hauser, M. G., & Kerr, F. J. 1989, ApJ, 336, 762
Stacy, G. J., Geis, N., Genzel, R., Lugten, J. B., Poglitsch, A., Sternberg, A., & Townes, C. H. 1991, ApJ, 373, 423
Stacey, G. J., Smyers, S. D., Kurtz, N. T., & Harwit, M. 1983a, ApJ, 265, L7
———. 1983b, ApJ, 268, L99
Stark, A. A., Davidson, J. A., Harper, D. A., Pernic, R., Loewenstein, R., Platt, S., Engargiola, G., & Casey, S. 1989, ApJ, 337, 650
Tielens, A. G. G. M., & Hollenbach, D. J. 1985, ApJ, 291, 722
Watson, W. D. 1972, ApJ, 176, 103
Wolfire, M. G., Hollenbach, D. J., & Tielens, A. G. G. M. 1989, ApJ, 344, 770
Wright, E. L. 1987, ApJ, 320, 818
Wright, E. L., et al. 1990, BAAS, 22, 874
Zmuidzinas, J., Betz, A. L., Boreiko, R. T., & Goldhaber, D. M. 1988, ApJ, 335, 774